The Company of Biologists

RESEARCH ARTICLE

Role of SmcHD1 in establishment of epigenetic states required for the maintenance of the X-inactivated state in mice

Yuki Sakakibara[1], Koji Nagao[2,*], Marnie Blewitt[3], Hiroyuki Sasaki[1], Chikashi Obuse[2] and Takashi Sado[1,4,*]

ABSTRACT

X inactivation in mammals is regulated by epigenetic modifications. Functional deficiency of SmcHD1 has been shown to cause de-repression of X-inactivated genes in post-implantation female mouse embryos, suggesting a role of SmcHD1 in the maintenance of X inactivation. Here, we show that de-repression of X-inactivated genes accompanied a local reduction in the enrichment of H3K27me3 in mouse embryonic fibroblasts deficient for SmcHD1. Furthermore, many of these genes overlapped with those having a significantly lower enrichment of H3K27me3 at the blastocyst stage in wild type. Intriguingly, however, depletion of SmcHD1 did not compromise the X-inactivated state in immortalized female mouse embryonic fibroblasts, in which X inactivation had been established and maintained. Taking all these findings together, we suggest that SmcHD1 facilitates the incorporation of H3K27me3 and perhaps other epigenetic modifications at gene loci that are silenced even with the lower enrichment of H3K27me3 at the early stage of X inactivation. The epigenetic state at these loci would, however, remain as it is at the blastocyst stage in the absence of SmcHD1 after implantation, which would eventually compromise the maintenance of the X-inactivated state at later stages.

KEY WORDS: X inactivation, Chromatin, Epigenetic modifications, Mouse development

INTRODUCTION

Female mammals, which have twice as many X-linked genes as males do, have evolved a mechanism to compensate for this dosage difference by inactivating one of the two X chromosomes during early development (Lyon, 1961). In the mouse, X inactivation is imprinted in favor of the paternal X chromosome in the extra-embryonic tissues, which give rise to the future placenta and some extra-embryonic membranes (Takagi and Sasaki, 1975), whereas it takes place in a random fashion (with respect to the parental origin of the X chromosome) in the embryonic tissue, which differentiates into all tissues of the fetus. In both imprinted and random X inactivation, silencing of the X chromosome is mediated by X-linked noncoding *Xist* RNA, which is monoallelically upregulated and coats the X chromosome from which it originates

in cis (Clemson et al., 1996; Marahrens et al., 1997; Panning and Jaenisch, 1996; Penny et al., 1996). Targeted disruption has clearly demonstrated that *Xist* is essential for X inactivation to occur in cis, and the X chromosome deficient for *Xist* never undergoes inactivation. It is well accepted that *Xist* RNA forms a platform or scaffold to recruit proteins involved in heterochromatinization or its maintenance on the X chromosome undergoing inactivation (Wutz, 2011). Once the inactivated state of the X chromosome is established, it is stably maintained throughout successive cell divisions in the somatic lineages. It is well known that epigenetic modifications such as DNA methylation and histone modifications play an important role in the stable maintenance of the inactivated state of the X chromosome (Wutz, 2011).

The importance of DNA methylation in the maintenance of X inactivation has been known for nearly four decades (Holliday and Pugh, 1975). CpG islands, which are often found in gene regulatory regions such as promoters or enhancers, are heavily methylated on the inactive X but less methylated on the active X. It has been shown that demethylation of CpG islands often leads to sporadic re-activation of genes on the inactive X, suggesting a role of DNA methylation in long-term memory for the stable maintenance of the repressed state. Roles of histone modifications in X inactivation have also been well studied. One of the most prominent features of the inactive X is the enrichment of histone H3 trimethylated at lysine 27 (H3K27me3), which is involved in gene repression and is a mark of facultative heterochromatin (Plath et al., 2003; Silva et al., 2004). Other histone modifications enriched on the inactive X include H2AK119ub1, H3K9me2, H3K9me3 and H4K20me1 (Chadwick and Willard, 2004; de Napoles et al., 2004; Fang et al., 2004; Heard et al., 2001; Keniry et al., 2016; Kohlmaier et al., 2004; Nozawa et al., 2013). In contrast, acetylated histone H3 and H4, both of which are involved in gene activation, are essentially excluded from the inactive X (Jeppesen and Turner, 1993). A role of H3K27me3 in the stable maintenance of the inactive X has been suggested in the extra-embryonic tissues of the mouse embryo based on studies of a loss-of-function mutation of Eed, which is one of the components in polycomb repressive complex 2 (PRC2) responsible for producing H3K27me3 (Wang et al., 2001). Female embryos carrying a paternal X-linked GFP transgene on an Eed-null background exhibit re-activation of the GFP transgene, which was repressed by imprinted X inactivation at earlier stages, in the extra-embryonic tissues.

SmcHD1 (structural maintenance of chromosomes containing hinge domain), a noncanonical member of the SMC family of proteins, was initially reported as a protein for which loss of function compromises X inactivation, resulting in female-specific lethality at the midgestation stage (Blewitt et al., 2008). The late timing of lethality suggested that SmcHD1 may be involved in the maintenance of X-linked gene silencing. In an SmcHD1-null mutant, *Smchd1*[MommeD1/MommeD1] (*Smchd1*[MD1/MD1] hereafter), re-activation of X-inactivated genes is often accompanied by

[1]Medical Institute of Bioregulation, Kyushu University, 3-1-1, Maidashi, Higashi-ku, Fukuoka, 812-8582, Japan. [2]Department of Biological Science, Graduate School of Science, Osaka University, Toyonaka, Japan. [3]The Walter and Eliza Hall Institute of Medical Research, 1G Royal Pde, Parkville 3052 VIC, Australia; The Department of Medical Biology, University of Melbourne, Parkville 3052, VIC, Australia. [4]Department of Advanced Bioscience, Graduate School of Agriculture, Kindai University, 3327-204, Nakamachi, Nara, 630-8505, Japan.

*Authors for correspondence (nagao@bio.sci.osaka-u.ac.jp; tsado@nara.kindai.ac.jp)

K.N., 0000-0003-1418-6988; T.S., 0000-0002-1232-0250

DEVELOPMENT

1

hypomethylation of their associated CpG islands, suggesting that SmcHD1 is involved in methylation of CpG islands on the inactive X (Blewitt et al., 2008). A subsequent study, however, showed that hypomethylation of CpG islands was not necessarily the sole basis for the de-repression of X-linked genes that had been silenced early on (Gendrel et al., 2012). More recently, we found that one of the heterochromatin protein 1 (HP1)-interacting proteins, termed HBiX1 (now known as LRIF1), associates with SMCHD1 in human cultured cells and suggested that the SMCHD1-HBiX1 complex plays a role in compaction of the Barr body representing the inactive X (Nozawa et al., 2013). Although these results suggest a role of SmcHD1 in chromatin regulation, how SmcHD1 exerts its effect on the stable repression of the inactive X is still obscure.

Here, we further study the effects of SmcHD1-deficiency on X inactivation in mouse embryos as well as its effects on embryonic development. We found that one of the reasons for female-specific lethality at the midgestation stages was likely to be the loss of the trophoblast giant cells between the maternal decidual tissues and spongiotrophoblast, which would cause deterioration of the proper exchange of materials between the mother and fetus. This suggests that trophoblast giant cells may be the most susceptible target of the misexpression of X-linked genes that have been inactivated early on. We also found that such misexpression occurred in mouse embryonic fibroblasts (MEFs), and was probably caused by local alterations of H3K27me3 and other histone modifications in addition to previously reported hypomethylation at CpG islands. Furthermore, many of the misexpressed genes overlapped with those showing a significantly low enrichment of H3K27me3 at the blastocyst stage in wild-type inner cell mass (ICM) and trophectoderm. Intriguingly, however, neither such alterations nor de-repression of X-inactivated genes were observed upon CRISPR/Cas9-mediated disruption of SmcHD1 in immortalized wild-type MEFs, in which X inactivation had been fully established and maintained. Based on these findings, we discuss the role of SmcHD1 in the process of X inactivation.

RESULTS
Smchd1$^{MD1/MD1}$ females exhibit a severe defect in the placenta
Although functional deficiency of SmcHD1 was initially reported to result in female-specific lethality at embryonic day (E) 10.5 (Blewitt et al., 2008), subsequent studies suggested that the phenotype of SmcHD1 deficiency could vary depending on the genetic background (Leong et al., 2013). Whereas half of males homozygous for Smchd1^{MD1} survive to weaning on the FVB/N background (Blewitt et al., 2005), those homozygous for a genetrap allele of Smchd1, another null mutation of Smchd1, die between E17.5 and weaning on the C57Bl/6 (B6) background (Leong et al., 2013). To evaluate the phenotype of Smchd1$^{MD1/MD1}$ mice on the B6 background, we backcrossed the Smchd1^{MD1} allele onto the B6 background for 20 generations. We then crossed males and females heterozygous for Smchd1^{MD1}. The results demonstrated that almost all males and females homozygous for Smchd1^{MD1} were lethal in utero (Table 1) although an exceptional male survived to term and

died a few days after birth. This lethality was consistent with the observations in mice carrying the genetrap allele on the B6 background (Leong et al., 2013). We then examined the gross morphology of Smchd1$^{MD1/MD1}$ embryos at E7.5, E10.5 and E13.5. Both male and female homozygotes were indistinguishable from wild-type and heterozygous littermates at E7.5 and E10.5. At E13.5, however, although homozygous males were apparently healthy with normal morphology, homozygous females exhibited clear developmental defects. Some of them had already died by the time of dissection and others were stunted and developmentally delayed as judged by limb morphology. In addition, we noticed that the placentas of homozygous females were in all cases smaller and thinner than those of healthy littermates (Fig. S1A). Histological examination revealed that whereas the spongiotrophoblast and labyrinthine trophoblast layers were formed fairly well, the trophoblast giant cells were barely present in the placentas of Smchd1$^{MD1/MD1}$ females (Fig. S1B). This was in strong contrast to the presence of the trophoblast giant cells in the placentas of homozygous males, which looked normal at E13.5 (Fig. S1A,B). A terminal deoxynucleotidyl transferase dUTP nick end labeling (TUNEL) assay further demonstrated that there was no significant difference between the wild-type and Smchd1$^{MD1/MD1}$ female placentas with respect to the number of cell deaths in the spongiotrophoblast or labyrinthine trophoblast (Fig. S1C). Our findings are consistent with the trophoblast giant cell defect observed in the Smchd1$^{MD1/MD1}$ female placenta on the FVB/N background (Blewitt et al., 2008). These findings taken together indicate that a loss of the trophoblast giant cells is likely to be at least one of the causes of the female-specific lethality of the homozygous mutants at around E13.5. In addition, these results suggest that the trophoblast giant cells are the predominant cell type that suffers from defects in X inactivation caused by the lack of SmcHD1.

X-linked genes become de-repressed gradually during development in Smchd1$^{MD1/MD1}$ embryos
Although the above results indicated that the lack of SmcHD1 impacted the development of the placenta, a previous study demonstrated that the X-linked GFP transgene on the inactivated X failed to be stably silenced in not only the extra-embryonic but also the embryonic tissues (Blewitt et al., 2008). To understand better the impact of SmcHD1-deficiency on X inactivation in the embryonic and extra-embryonic tissues, two-color RNA fluorescence in situ hybridization (RNA-FISH) was carried out to assess the expression of Xist and another X-linked gene, Atrx, in E7.5 embryos. When the distal part of the embryo, which is enriched in embryonic ectoderm, was examined, a pinpoint Atrx signal was detected in the Xist cloud, indicating misexpression of Atrx on the inactive X, in 4% and 21% of the nuclei in wild-type and Smchd1$^{MD1/MD1}$, respectively (Fig. 1A,B). By contrast, in the trophoblast, which is part of the extra-embryonic tissue, 70% of the nuclei showed such misexpression of Atrx in Smchd1$^{MD1/MD1}$, whereas only 25% did so in wild type (Fig. 1A,B). Relatively more nuclei with misexpression of Atrx were observed in the trophoblast, even in the wild type, consistent with the sporadic reactivation of X-inactivated genes reported previously (Corbel et al., 2013; Hadjantonakis et al., 2001). Nonetheless, it was intriguing that in the mutants, Atrx was misexpressed in a much larger fraction of the nuclei in the trophoblast than in the distal part of the embryo. This is consistent with the finding that the trophoblast is a prominently affected tissue in the Smchd1$^{MD1/MD1}$ placenta.

It has been suggested that SmcHD1-deficient embryos can initiate X inactivation but fail to maintain the inactivated state.

Table 1. Number of pups obtained from a cross between males and females heterozygous for Smchd1^{MD1}

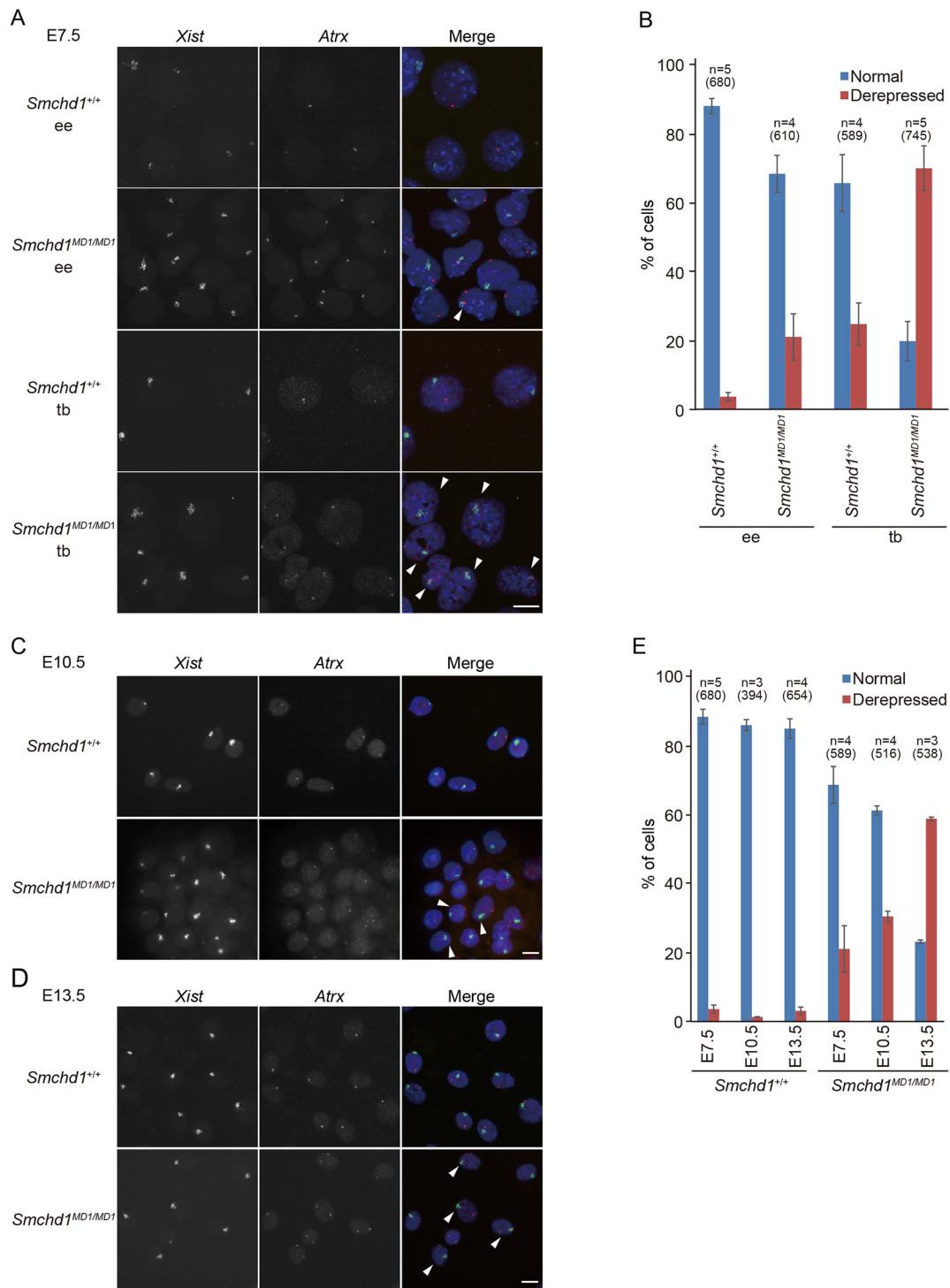|	Females	Males	Total
Smchd1$^{+/+}$	52 (18.3%)	54 (19.0%)	106 (37.3%)
Smchd1$^{MD1/+}$	89 (31.3%)	88 (31.0%)	171 (62.3%)
Smchd1$^{MD1/MD1}$	0 (0%)	1 (0.4%)	1 (0.4%)
Total	141	143	284

DEVELOPMENT

Fig. 1. The X-linked *Atrx* gene was gradually de-repressed in the absence of SmcHD1 during development. (A) Images of RNA-FISH detecting *Xist* (green) and *Atrx* (red) expression in the embryonic ectoderm (ee) and trophoblast (tb) of E7.5 *Smchd1*^{+/+} and *Smchd1*[MD1/MD1] embryos. Arrowheads indicate the nuclei showing misexpression of *Atrx* in the *Xist* cloud. Nuclei were counterstained with DAPI. (B) Summary of the RNA-FISH in A showing the prevalence of nuclei with monoallelic (normal) and biallelic (de-repressed) *Atrx* expression. At least 100 nuclei were examined. *n*, the number of embryos or independently prepared primary MEFs. The total numbers of cells examined are shown in the parentheses. (C,D) RNA-FISH to examine *Xist* (green) and *Atrx* (red) expression in MEFs prepared from E10.5 (C) and E13.5 (D) fetuses. Arrowheads indicate nuclei with misexpression of *Atrx*. (E) The prevalence of nuclei with monoallelic (normal) and biallelic (de-repressed) *Atrx* expression at the indicated stage (more than 100 randomly selected nuclei were evaluated in each case). *n*, the number of embryos or independently prepared primary MEFs. The total numbers of cells examined are shown in the parentheses. Error bars represent s.d. Scale bars: 10 µm.

This would predict that the population of nuclei with misexpression of *Atrx* in the *Xist* cloud, although as low as 21% in the mutant embryonic tissues at E7.5, would increase when examined at later stages. To examine whether this was the case, we took advantage of primary MEFs prepared from E10.5 and E13.5 fetuses for RNA-FISH. Two-color RNA-FISH demonstrated that whereas misexpression of *Atrx* was found in 1% and 3% of E10.5 and E13.5 wild-type MEFs, respectively, such misexpression was found

in 31% and 59% of E10.5 and E13.5 $Smchd1^{MD1/MD1}$ MEFs, respectively (Fig. 1C-E). These results suggest that genes on the inactive X become gradually de-repressed during embryonic development in the absence of SmcHD1.

Wide de-repression of genes on the inactive X in E13.5 $Smchd1^{MD1/MD1}$ MEFs

To examine the extent to which the genes on the inactive X were de-repressed, we carried out allele-specific RNA-seq using E13.5 wild-type and $Smchd1^{MD1/MD1}$ MEFs, in which one X ($X^{\Delta\Delta}$) harbors a null mutation of $Xist$ ($Xist^{\Delta\Delta}$) and the other X (X^{JF1}) is derived from the JF1 strain. As $X^{\Delta\Delta}$ never undergoes inactivation during the process of X inactivation (Hoki et al., 2009), X^{JF1} alone is inactivated in $X^{\Delta\Delta}X^{JF1}$ MEFs. The appearance of X-encoded reads containing JF1-type single nucleotide polymorphisms (SNPs) or insertions and deletions (INDELs), therefore, indicates de-repression of genes on X^{JF1}. The allelic probability of 419 informative genes on X^{JF1} was calculated by simply dividing the number of JF1-reads by total allele-specific reads, and was plotted according to the probability of the respective genes on X^{JF1} in [$X^{\Delta\Delta}X^{JF1}$; $Smchd1^{MD1/MD1}$] MEFs, with the lower probability on the left and higher on the right (Fig. 2A). Those genes on X^{JF1} with an allelic probability of 0.1 or higher in $X^{\Delta\Delta}X^{JF1}$ were classified as escapees. As shown in Fig. 2A,B, it was evident that the great majority of the genes on X^{JF1} were substantially repressed in $X^{\Delta\Delta}X^{JF1}$ MEFs, as expected. In contrast, although 48% of the genes were stably repressed, the remaining 52% were de-repressed at various levels in [$X^{\Delta\Delta}X^{JF1}$; $Smchd1^{MD1/MD1}$] MEFs. These overall differences could be due to either differences in the extent of de-repression among individual genes or to differences in the proportion of cells that de-repress individual genes, or both. The de-repressed genes did not show a bias in their distribution regarding the chromosomal position relative to the $Xist$ locus on X^{JF1} but tended to be located in gene-dense regions (Fig. 2C,D). In addition, they often overlapped with genes that manifested relatively higher expression levels in $X^{\Delta\Delta}X^{JF1}$ (Fig. 2D). Expression levels of the escapees were slightly upregulated in [$X^{\Delta\Delta}X^{JF1}$; $Smchd1^{MD1/MD1}$] MEFs compared with those in $X^{\Delta\Delta}X^{JF1}$ (Fig. 2B). This might be an indication that the overall chromatin state of X^{JF1} in [$X^{\Delta\Delta}X^{JF1}$; $Smchd1^{MD1/MD1}$] MEFs is not as condensed as that in $X^{\Delta\Delta}X^{JF1}$. Nonetheless, it was evident that genes widely distributed on the inactivated X^{JF1} were de-repressed in the absence of SmcHD1. We also examined the relationship between the expression levels of de-repressed X-linked genes and their Xi probability. As shown in Fig. 2E, the misregulated genes were distributed roughly along the red curve representing the predicted relationship between the allelic probability of X^{JF1} genes and their total expression levels in [$X^{\Delta\Delta}X^{JF1}$; $Smchd1^{MD1/MD1}$] MEFs relative to $X^{\Delta\Delta}X^{JF1}$, assuming the expression levels of those genes on the active $X^{\Delta\Delta}$ is the same between these MEFs. This indicates that the excess expression of the X-linked genes in [$X^{\Delta\Delta}X^{JF1}$; $Smchd1^{MD1/MD1}$] MEFs is essentially derived from X^{JF1}.

We compared the X-linked genes de-repressed in [$X^{\Delta\Delta}X^{JF1}$; $Smchd1^{MD1/MD1}$] MEFs with those misexpressed from the X chromosome harboring the $Xist^{CAG\Delta5'}$ allele ($X^{CAG\Delta5'}$) (Sakata et al., 2017), which expresses mutated $Xist$ RNA lacking the A-repeat, and is therefore defective in gene silencing despite its coating the X chromosome, in the E7.5 trophoblast. Although the cell lineage and mode of X inactivation are distinct between MEFs and the trophoblast, it would still be of interest to examine whether there is correlation between genes that fail to be repressed due to the defect in the initiation of X inactivation and those de-repressed due

to the failure of the maintenance of X inactivation. Fig. 2F shows that many of the genes misexpressed from the inactive X in [$X^{\Delta\Delta}X^{JF1}$; $Smchd1^{MD1/MD1}$] MEFs (Xi probability ≥0.1) are common to those misexpressed from $X^{CAG\Delta5'}$ in [$X^{JF1}X^{CAG\Delta5'}$; $Smchd1^{+/+}$] trophoblast (Xi probability ≥0.1) although their Xi probabilities were rather variable. Of 283 non-escapee genes informative in both data sets, 164 were de-repressed in both [$X^{JF1}X^{CAG\Delta5'}$; $Smchd1^{+/+}$] trophoblast and [$X^{\Delta\Delta}X^{JF1}$; $Smchd1^{MD1/MD1}$] MEFs (Fig. 2G), suggesting a link between genes that failed to be silenced by dysfunctional $Xist^{CAG\Delta5'}$ RNA and those that failed to be stably silenced in the absence of SmcHD1.

Replication timing of the inactive X shifts early-mid S phase in $Smchd1^{MD1/MD1}$ female MEFs

The finding that the inactivated X chromosome was globally de-repressed in E13.5 female MEFs deficient for SmcHD1 prompted us to examine replication timing of the X chromosomes. It is well known that whereas the active X replicates synchronously with other autosomes throughout S phase, replication of the inactive X is confined to late in S phase, as is the case for other heterochromatin regions. To examine the replication timing of the X chromosomes, E7.5 embryos and MEFs prepared from E10.5 and E13.5 fetuses were allowed to incorporate bromodeoxyuridine (BrdU) and chromosome spreads were subsequently stained with Acridine Orange. We found that although one of the two X chromosomes in wild type exhibited typical asynchronous replication in essentially all cells of a distal part of E7.5 embryos (100%) and E10.5 and E13.5 MEFs (98-100%), the proportion of cells with two synchronously replicating X chromosomes was 2% in the distal part of E7.5 embryos, and it gradually increased to 25% of E10.5 MEFs, and further to 55% of E13.5 MEFs (Fig. 3). This result suggests that re-activation of X-inactivated genes accompanies a shift of timing of replication of the inactivated X chromosome from late to early-mid S phase during development of $Smchd1^{MD1/MD1}$ female embryos.

A reduction in H3K27me3 levels correlates with de-repression of X-linked genes in $Smchd1^{MD1/MD1}$ MEFs

A previous study showed that loss of SmcHD1 results in hypomethylation of some X-linked CpG islands but does not affect the enrichment of H3K27me3 on the inactive X chromosome as determined by immunofluorescence in the embryo (Blewitt et al., 2008). Other histone modifications specific for the inactive X, such as H2AK119ub (de Napoles et al., 2004; Fang et al., 2004), H3K9me2 (Heard et al., 2001) and H4K20me1 (Schotta et al., 2008), have not, however, been studied so far. Accordingly, we examined the E13.5 wild-type and $Smchd1^{MD1/MD1}$ female MEFs analyzed above for immunofluorescence using antibodies against H2AK119ub, H3K9me2 and H4K20me1 in combination with an antibody against H3K27me3. The majority of nuclei in both wild-type and SmcHD1-deficient MEFs exhibited colocalization of H2AK119ub and H3K9me2 with H3K27me3 (Fig. S2B,C,E). The proportion of nuclei showing colocalization of H4K20me1 with H3K27me3, in contrast, was as low as 30% in both wild-type and SmcHD1-deficient cells (Figs S2D,E). These results demonstrated that despite the de-repression of X-inactivated genes and a shift of the replication timing of the hitherto inactive X chromosome, the enrichment of the respective histone modifications specific for the inactive X was apparently not affected on the de-repressed X chromosome in SmcHD1-deficinet MEFs.

Although immunofluorescence analyses revealed no significant difference in histone modifications on the inactive X between wild-type and $Smchd1^{MD1/MD1}$ female MEFs, it was possible that there
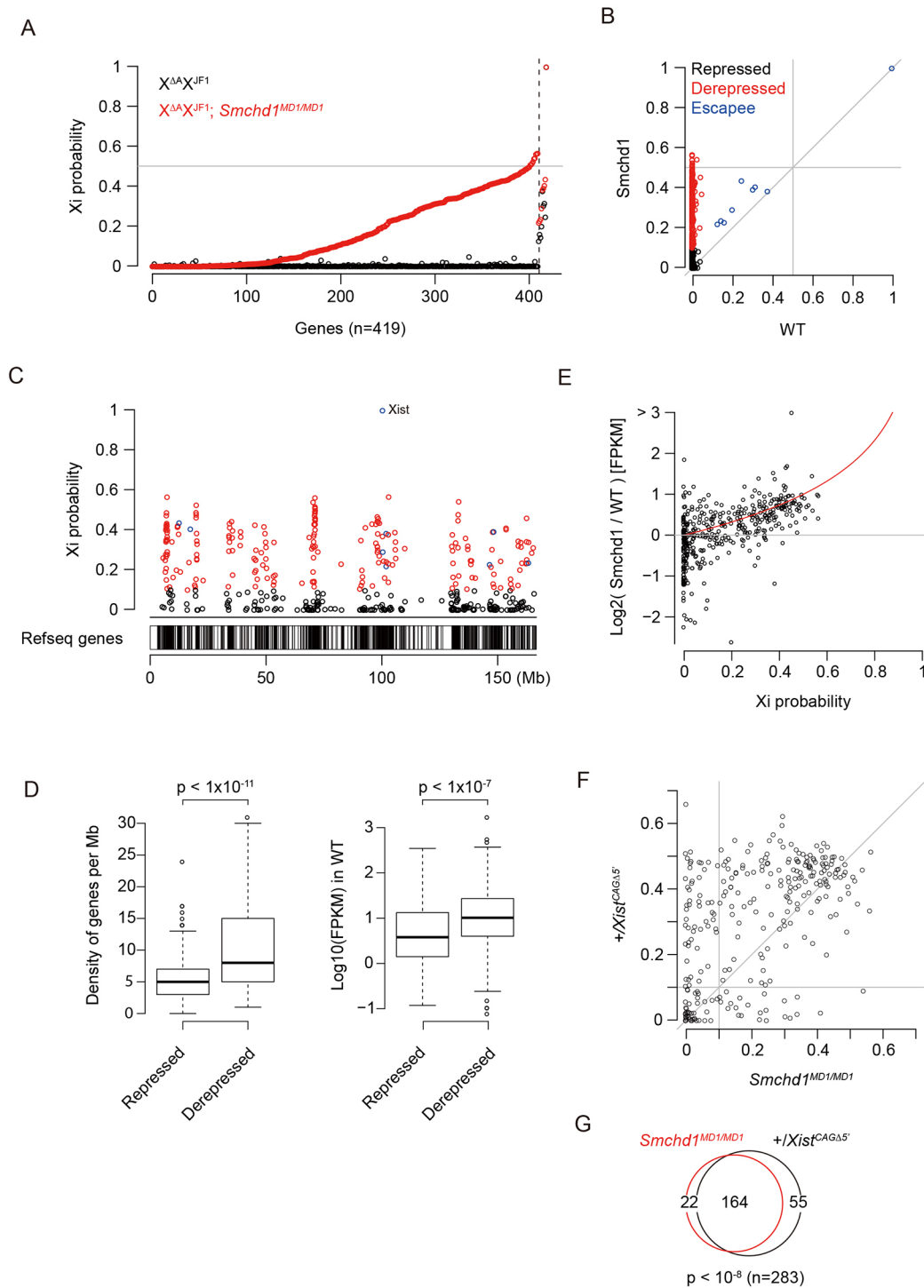
Fig. 2. See next page for legend.

were some local alternations in their distribution that could be detected if closely examined along the chromosome. To address this issue, we carried out chromatin immunoprecipitation combined with sequencing (ChIP-seq) analysis for the H3K27me3 status in E13.5 MEFs and made a detailed analysis of the distribution of H3K27me3 on the X chromosome. Fig. 4A shows the distribution of H3K27me3 in a 5-Mb region spanning the *Atrx* locus on the X chromosome in wild-type and *Smchd1^{MD1/MD1}* MEFs along with the position of protein-coding genes present in this region and Xi probability in *Smchd1^{MD1/MD1}* MEFs. Whereas H3K27me3 was

uniformly distributed with the exception of escapee loci (5530601H04Rik and Pbdc1) in wild-type MEFs, a local reduction in the enrichment of H3K27me3 was evident at the de-repressed loci in *Smchd1^{MD1/MD1}* MEFs. These loci included the *Atrx* locus, which we found was gradually de-repressed in SmcHD1 mutants (Fig. 4A). A number of loci de-repressed on the X chromosome in SmcHD1-deficient MEFs manifested a similar reduction in the enrichment of H3K27me3. The non-escapee genes were plotted according to their Xi probability and the enrichment of H3K27me3 in *Smchd1^{MD1/MD1}* MEFs (Fig. 4B), and the plot

Fig. 2. Widely distributed genes were de-repressed on the inactive X in E13.5 *Smchd1^MD1/MD1* MEFs. (A) Xi probability (allelic probability of X^JF1) of 419 informative X-linked genes was compared between X^ΔΔX^JF1 and [X^ΔΔX^JF1; *Smchd1^MD1/MD1*] MEFs. First, genes were divided into non-escapees and escapees (the boundary is shown as a dashed line) according to the Xi probability in X^ΔΔX^JF1 MEFs, and subsequently ranked by the Xi probability in [X^ΔΔX^JF1; *Smchd1^MD1/MD1*] MEFs, with a lower value on the left and a higher value on the right. Informative X-linked genes were classified as follows: escapees, genes with Xi probability ≥0.1 in X^ΔΔX^JF1 MEFs; repressed genes, non-escapees with Xi probability <0.1 in [X^ΔΔX^JF1; *Smchd1^MD1/MD1*] MEFs; de-repressed genes, otherwise. (B) Scatter plot analysis of the Xi probability analyzed in A between X^ΔΔX^JF1 and [X^ΔΔX^JF1; *Smchd1^MD1/MD1*] MEFs. Escapees, repressed and de-repressed genes are shown in blue, black and red, respectively. (C) Distribution of the 419 genes analyzed in A on the X chromosome in [X^ΔΔX^JF1; *Smchd1^MD1/MD1*] MEFs. Color schema as in B. (D) Left: whether the genes on Xi are repressed or not in [X^ΔΔX^JF1; *Smchd1^MD1/MD1*] MEFs correlates with the density of expressed genes (FPKM ≥1 in X^ΔΔX^JF1 MEFs). The gene densities were compared between repressed and de-repressed genes. Right: whether the genes on Xi are silenced or not in [X^ΔΔX^JF1; *Smchd1^MD1/MD1*] MEFs correlates with their expression levels in X^ΔΔX^JF1 MEFs (wild type). De-repressed genes manifest higher expression than those genes that stay repressed. Significance of the difference was evaluated by the Wilcoxon test (215 de-repressed and 195 repressed genes). Solid bars represent the median; box extends from the 25th to the 75th percentile; whiskers extend to the most extreme data point no more than 1.5 times the interquartile range from the box. (E) Xi probability and the expression levels of 410 non-escapees in [X^ΔΔX^JF1; *Smchd1^MD1/MD1*] MEFs relative to X^ΔΔX^JF1 (wild type) are plotted. The red curve indicates an ideal relationship between Xi probability and the corresponding expression levels relative to wild type, assuming the expression levels of X^ΔΔ genes are not affected. (F) Xi probability in [X^ΔΔX^JF1; *Smchd1^MD1/MD1*] MEFs was compared with the allelic probability of genes on X carrying *Xist^CAGΔ5′* in the [X^JF1X^CAGΔ5′; *Smchd1^+/+*] trophoblast. Values for non-escapee genes informative in both data sets were plotted (*n*=283), and those with an allelic probability of more than 0.1 were referred to as de-repressed genes. (G) Venn diagram comparing the number of genes de-repressed in *Xist*-coated X chromosome between [X^ΔΔX^JF1; *Smchd1^MD1/MD1*] MEFs and [X^JF1X^CAGΔ5′; *Smchd1^+/+*] trophoblast. *P*-value is based on the hypergeometric test.

Fig. 3. Replication timing of the inactive X shifts to earlier than late S phase in *Smchd1^MD1/MD1*. (A) Chromosome spreads of E13.5 MEFs after incorporation of BrdU and subsequent staining with Acridine Orange. Arrow indicates an asynchronously replicating X chromosome and arrowheads indicate a synchronously X chromosome. (B) Percentage of cells containing one asynchronously replicating X chromosome and two synchronously X chromosomes in E7.5 embryos and E10.5 and E13.5 MEFs of wild-type and *Smchd1^MD1/MD1* mutants. More than 20 chromosome spreads were examined for E7.5 and E10.5 embryos and 30 were examined for E13.5 MEFs. *n*, the number of embryos or independently prepared primary MEFs. The total number of cells examined are shown in the parentheses. Error bars represent s.d. Scale bar: 10 μm.

demonstrated that the genes with a higher Xi probability generally manifested a lower enrichment of H3K27me3 than the same gene set in wild-type MEFs.

We also took advantage of a methyl-binding domain sequencing (MBD-seq) data set (Gendrel et al., 2012) to analyze the Xi probability of genes associated with methylated and unmethylated CpG islands (CGIs) in *Smchd1^MD1/MD1* MEFs. As shown in Fig. 4C, the Xi probability of genes associated with unmethylated CGIs was significantly higher than that of genes associated with methylated ones in *Smchd1^MD1/MD1* MEFs. Gendrel et al. demonstrated that whereas methylation of fast-methylating CGIs (class A and B) on the inactive X is independent of SmcHD1, methylation of slow-methylating CGIs (class C) depends on SmcHD1. When the Xi probability was compared between genes associated with such fast- and slow-methylating CGIs, the latter group of genes manifested a significantly higher Xi probability than the former in *Smchd1^MD1/MD1* MEFs (Fig. 4D). These results are consistent with the idea that SmcHD1-dependent CGIs are involved in stable repression of X-linked genes.

Many of the X-linked genes de-repressed in *Smchd1^MD1/MD1* MEFs overlap with those characterized by a lower enrichment of H3K27me3 in wild-type blastocysts

The finding that the enrichment of H3K27me3 was diminished at de-repressed X-linked gene loci in *Smchd1^MD1/MD1* MEFs prompted us to examine further the epigenetic state of such gene loci at an earlier developmental stage in the normal context. We took advantage of previously published ChIP-seq data of H3K27me3 at the blastocyst stage (Liu et al., 2016) and queried the H3K27me3
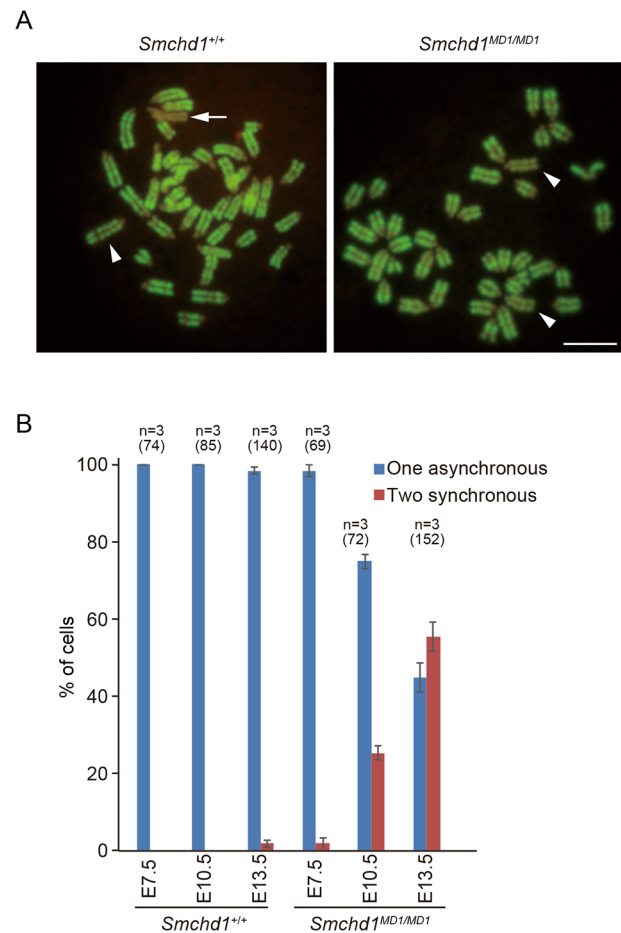
state of the ICM cells and trophectoderm at the X-linked gene loci stably repressed as well as those de-repressed in *Smchd1^MD1/MD1* MEFs. Of note, the ICM in this dataset showed no sign of X chromosome re-activation because the H3K27me3 status was indistinguishable between the ICM and trophectoderm. As shown in Fig. 5A, de-repressed X-linked genes exhibited a significantly lower enrichment of H3K27me3 in the ICM cells and trophectoderm compared with stably repressed X-linked genes in the respective cell types. We then examined the allele-specific expression status in the pre-implantation and early post-implantation stage embryos (Borensztein et al., 2017a,b). Fig. 5B compares a paternal probability between two classes of the X-linked genes, which either stay repressed or become de-repressed in *Smchd1^MD1/MD1* MEFs. The former shows a clear decrease in a paternal probability during pre-implantation development from four-cell to ICM of the blastocyst, reflecting inactivation of the paternal X. In contrast, those genes that become de-repressed manifest a significantly higher paternal probability in the ICM, epiblast, and primitive endoderm cells than those that stayed
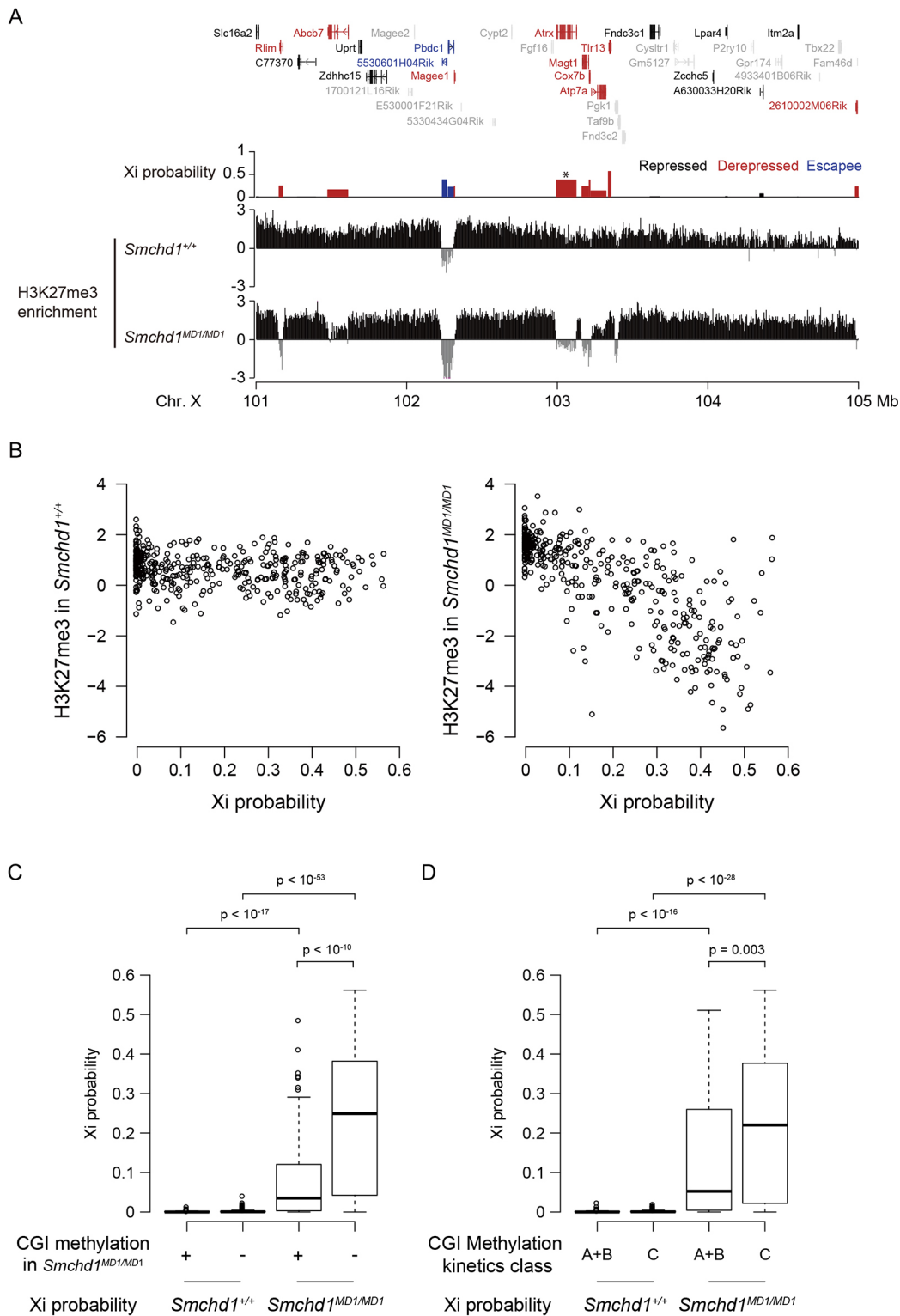
Fig. 4. Correlation between gene expression and histone modification on the X chromosome in *Smchd1*[MD1/MD1] MEFs. (A) Log2-transformed H3K27me3 enrichment over input per 5-kb bin revealed by ChIP-seq in a genomic region containing an escapee (blue) as well as both repressed (black) and de-repressed (red) genes in parallel with the modes of their expression from the Xi in $X^{\Delta A}X^{JF1}$; *Smchd1*[MD1/MD1]. Genes with uninformative Xi probabilities are shown as gray. The Xi probability of *Atrx* is indicated by asterisk. (B) Correlation between Xi probability and log2-transformed H3K27me3 enrichment of its gene body over input in *Smchd1*^{+/+} (left) and *Smchd1*[MD1/MD1] (right) MEFs for 408 informative non-escapee genes. (C) Correlation between CGI methylation levels in *Smchd1*[MD1/MD1] MEFs (Gendrel et al., 2012) and Xi probability. The methylated class is the combined class of methylated and intermediate CGIs in *Smchd1*[MD1/MD1] MEFs defined by Gendrel et al. (2012). Eighty-eight and 220 genes were classified into the methylated (+) and unmethylated (−) classes, respectively. (D) Correlation between CGI methylation kinetics in differentiating XX embryonic stem cells (Gendrel et al., 2012) and Xi probability. Class A+B (n=74) and C (n=126) genes are associated with fast- and slow-methylating CGIs, respectively, according to the definition by Gendrel et al. (2012). Significance of the difference was evaluated by the Wilcoxon test in C and D. In C and D, solid bars represent the median; box extends from the 25th to the 75th percentile; whiskers extend to the most extreme data point no more than 1.5 times the interquartile range from the box.
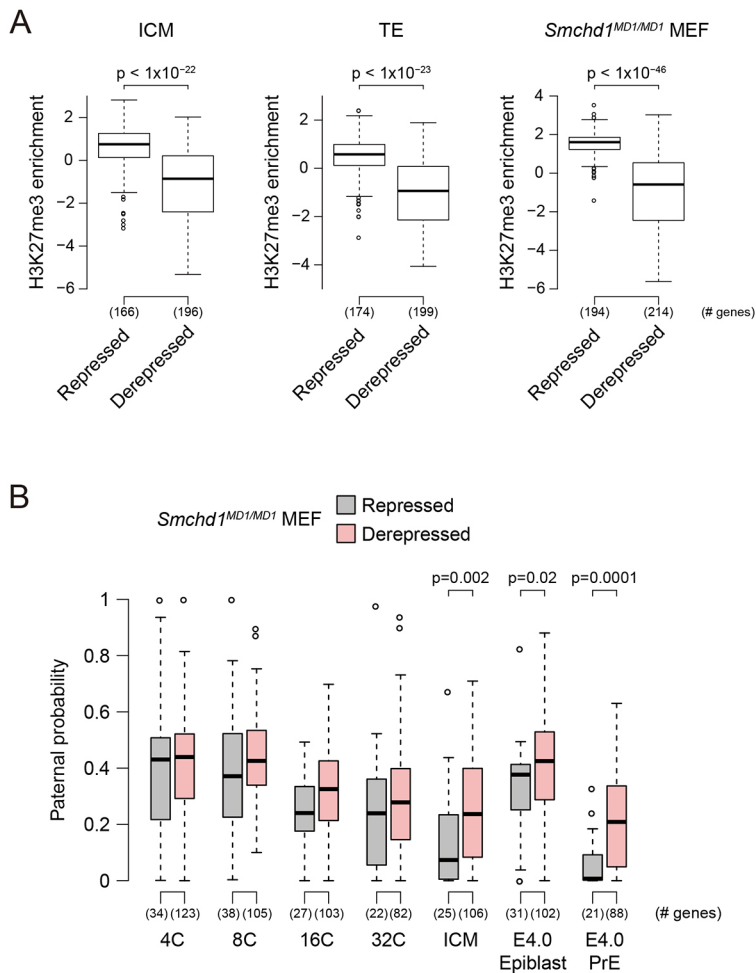
Fig. 5. Many of the de-repressed X-linked genes represent those characterized by a lower enrichment of H3K27me3 and higher Xi probability at the blastocyst stage. (A) Log2-transformed H3K27me3 enrichment in ICM and trophectoderm (TE) obtained from Liu et al. (2016) as well as in *Smchd1*[MD1/MD1] MEFs are compared between the repressed and de-repressed genes in *Smchd1*[MD1/MD1] MEFs. Significance of the difference was evaluated by the Wilcoxon test. The number of genes with informative H3K27me3 enrichment is indicated in brackets. (B) The mean of allele-specific expression ratios among single cells in 4- to 32-cell stages (4C-32C), E3.5 ICM, E4.0 epiblast, and E4.0 primitive endoderm (PrE) obtained from Borensztein et al. (2017a,b) are compared as in A. In A and B, solid bars represent the median; box extends from the 25th to the 75th percentile; whiskers extend to the most extreme data point no more than 1.5 times the interquartile range from the box.

repressed (Fig. 5B), consistent with a lower enrichment of H3K27me3 in ICM and trophectoderm. This result suggests that these de-repressed genes represent those that had been incompletely silenced at the blastocyst stage and/or preferentially reactivated thereafter due to a lack of sufficient H3K27me3, and perhaps other epigenetic modifications. This finding raises an intriguing possibility that those genes characterized by a lower enrichment of H3K27me3 at the blastocyst stage fail to acquire additional H3K27me3 during post-implantation development in *Smchd1*[MD1/MD1] embryos, resulting in their de-repression at later stages.

SmcHD1 is dispensable for the maintenance of X inactivation once the inactive state has been established

The results obtained so far suggested that the apparent failure of the maintenance of the X-inactivated state in the SmcHD1 mutants could be ascribed to defects in the proper establishment of epigenetic modifications such as CpG methylation and H3K27me3. We therefore examined whether SmcHD1 was required for the maintenance of the X-inactivated state in cells in which X inactivation had been substantially established and maintained. For this, we employed CRISPR/Cas9-mediated genome editing to disrupt the *Smchd1* gene in immortalized female MEFs prepared from E13.5 fetuses (Fig. 6A). We successfully obtained two independent lines with disruption of both *Smchd1* alleles, which were referred to as KO1 and KO2. DNA sequencing revealed a one-base deletion on one allele and a two-base deletion on the other in KO1 and four-base deletions on both

alleles in KO2. Western blotting confirmed the absence of SmcHD1 protein in both lines (Fig. 6B). These two KO cell lines and the original immortalized female MEFs were examined for the expression of *Atrx* as well as *Xist* by RNA-FISH. In contrast to the MEFs derived from *Smchd1*[MD1/MD1] fetuses, *Atrx* in KO1 and KO2 MEFs stayed repressed on the *Xist*-coated X chromosome, as in the original immortalized MEFs (Fig. 6C,D). This result suggested that genes on the inactive X in KO1 and KO2 MEFs were stably repressed in the absence of SmcHD1. In addition, the replication timing of the inactive X was not affected in the knockout MEFs (Fig. 6E,F). We further studied the epigenetic states of X-linked genes that stay repressed in KO1 and KO2 MEFs. Quantitative PCR following ChIP for H3K27me3 demonstrated that a lower enrichment of H3K27me3 was evident at both the *Atrx* and *Hprt* loci in primary MEFs prepared from a fetus deficient for SmcHD1 than in those prepared from a wild-type fetus (Fig. 6G), consistent with the results of ChIP-seq. In contrast, a reduction in the enrichment of H3K27me3 was moderate in immortalized MEFs depleted for SmcHD1 compared with immortalized parental wild-type MEFs. This suggests that depletion of SmcHD1 in cells that have established and stably maintain an X-inactivated state has only a moderate impact on the H3K27me3 state of the inactive X. We also carried out bisulfite sequencing (Fig. S3). Methylation levels at three X-linked loci, *Atrx*, *Hprt* and *Mtm1*, were relatively low (up to 20%) even in wild-type MEFs regardless of their being immortalized or not. These loci in primary MEFs deficient for SmcHD1, however, manifested much lower levels of methylation
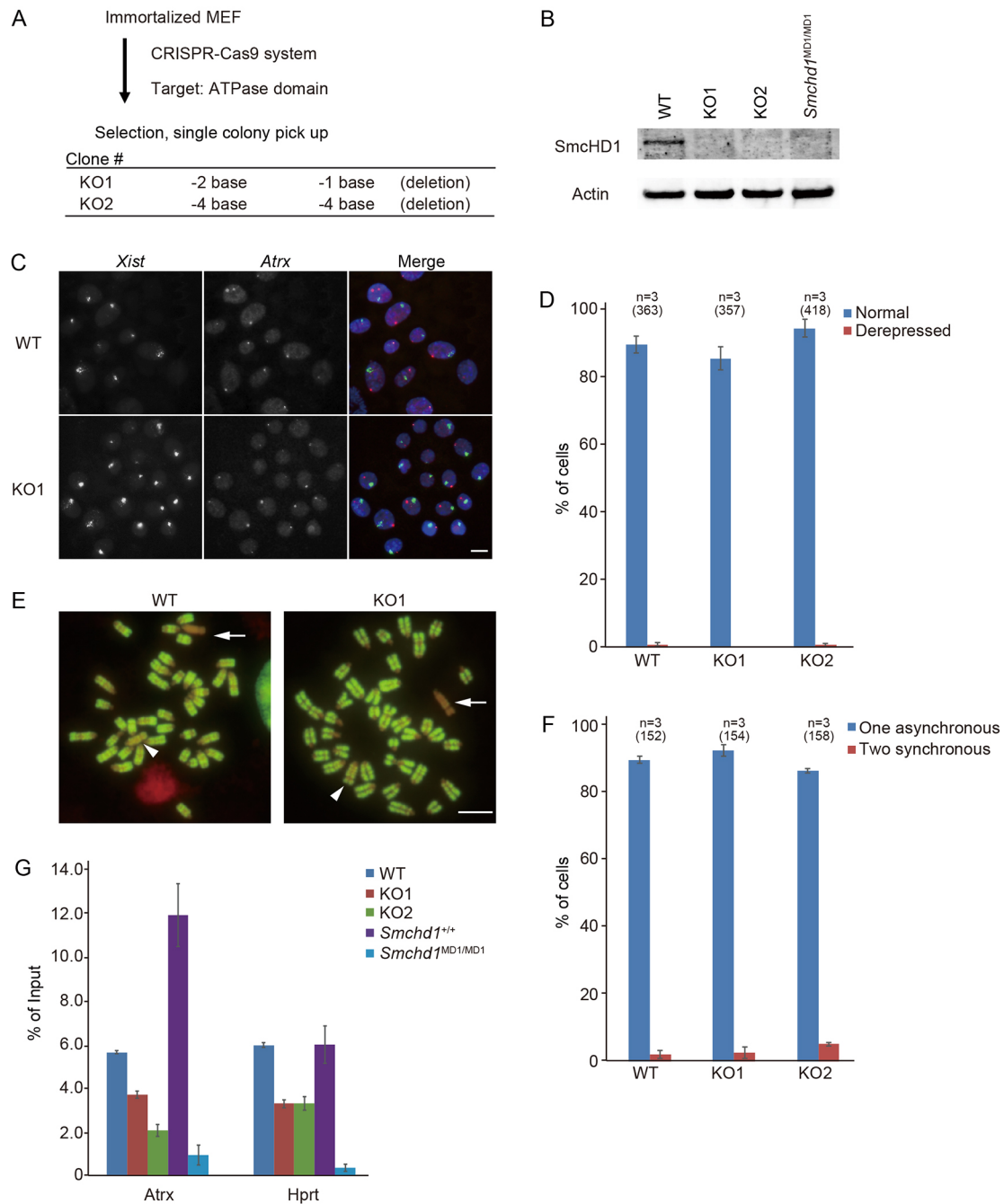
Fig. 6. SmcHD1 is not required for stable maintenance of the X-inactivated state once X chromosome inactivation has been established. (A) Strategy for knocking out *Smchd1* using the CRISPR/Cas9 system. (B) Successful depletion of SmcHD1 was confirmed by western blotting in KO1 and KO2. Whole cell extracts prepared from wild-type (WT), KO1, KO2 and *Smchd1$^{MD1/MD1}$* MEFs were examined. Actin served as a loading control. (C) Expression of *Xist* (green) and *Atrx* (red) was examined by RNA-FISH in WT and KO1 MEFs. Nuclei were counterstained with DAPI. (D) Histogram shows percentage of the nuclei with normal (monoallelic) and de-repressed (biallelic) state of *Atrx* expression in WT, KO1 and KO2 (more than 100 randomly selected nuclei were counted in each case). *n*, the number of experiments. The total number of cells examined are shown in the parentheses. (E) Replication timing of each X chromosome was examined in WT, KO1 and KO2. Arrowheads indicate synchronously replicating X chromosomes, and arrows indicate late-replicating X chromosomes. (F) A histogram showing the percentage of the chromosome spreads with one asynchronously replicating X and two synchronously replicating X chromosomes in each of WT, KO1 and KO2 MEFs (more than 100 randomly selected chromosome spreads were counted in each case). (G) Enrichment of H3K27me3 at *Atrx* and *Hprt* were examined by qPCR following ChIP. Primary MEFs prepared from E13.5 wild-type and *Smchd1$^{MD1/MD1}$* fetuses were included in the assay. Error bars represent s.d. Scale bars: 10 μm.

(0-7%) than those in wild-type primary MEFs, consistent with a previous study by Blewitt et al. (2008). In contrast, depletion of SmcHD1 did not result in hypomethylation to that extent and had only a moderate impact again in immortalized MEFs. This result suggested that although SmcHD1 was required for methylation of X-linked genes during the X inactivation process, it apparently had a minor influence on the maintenance of this methylation pattern. These findings suggested that the reversibility of the X-inactivated state is different between primary MEFs derived from female fetuses lacking SmcHD1 and cells depleted for SmcHD1 after X inactivation has been substantially established. It is therefore likely that although SmcHD1 is dispensable for the stable maintenance of

the X-inactivated state once it is established, SmcHD1 plays a role in establishing the proper epigenetic modifications required for the stable maintenance of the X-inactivated state later on.

DISCUSSION

Placental defect apparently contributes to female-specific lethality of SmcHD1 mutants at the midgestation stages

Although homozygous mutation of SmcHD1 was initially reported to cause female-specific embryonic lethality at midgestation stages, a subsequent study revealed that males were also perinatal lethal on the B6 background. Morphological anomaly of homozygous females becomes evident at around E13.5, with placental hypoplasia. Histological analysis demonstrated that trophoblast giant cells located between the maternal decidual tissue and spongiotrophoblast in homozygous males as well as wild-type females were missing in homozygous females. The lack of trophoblast giant cells would cause malfunction of the placenta and subsequent lethality of the females at the midgestation stages. A partial loss-of-function mutation of the *Xist* gene, *Xist^{IVS}*, which we previously reported, also results in failure to maintain the X-inactivated state in the placental tissues when paternally inherited (Hoki et al., 2011). Trophoblast giant cells are also the tissue that is most strongly affected in that case. It is therefore reasonable to conclude that the trophoblast giant cells are the tissue most susceptible to deleterious effects of de-repression of X-inactivated genes. Females homozygous for the SmcHD1 mutation and those carrying paternal *Xist^{IVS}* are, in fact, phenotypically similar, which suggests that there may be a functional relationship between these two mutations.

Genes de-repressed on the inactive X in the absence of SmcHD1

Among the 419 informative X-linked genes examined, more than half were de-repressed in female MEFs lacking functional SmcHD1. Although these genes manifest generally high expression when carried on the active X in wild-type, those that stay repressed even in the absence of SmcHD1 manifest generally low expression. It is possible that genes highly expressed on the active X would require robust repressive modifications for stable silencing on the X chromosome once inactivated, and such a chromatin state may not be established in the absence of SmcHD1. Incomplete repressive modifications thus formed, however, might still be sufficient to prevent de-repression of weakly expressed genes on the inactivated X. It was of interest to find that many of the genes de-repressed on the inactive X in female MEFs deficient for SmcHD1 are largely common to those that fail to be silenced by dysfunctional *Xist$^{CAGΔ5'}$* RNA in trophoblast cells. This suggests that among the X-linked genes that are subject to inactivation, some are readily silenced and others are not, and it would be relatively easy for the latter genes to become de-repressed on the inactivated X if its epigenetic state were not properly established. It is likely that genes on the X chromosome respond differentially to the wave of inactivation depending on their expression level.

Role of SmcHD1 in the establishment of the X inactivation process

Blewitt et al. previously showed using an X-linked GFP transgene that the fluorescence of GFP, which was initially diminished by X inactivation, gradually re-appeared during development in *Smchd1$^{MD1/MD1}$* females (Blewitt et al., 2008). Although this looks like a defect in the maintenance of X inactivation, it does not necessarily exclude other possibilities, such as an incomplete establishment of the X-inactivated state. A lack of the establishment of the proper epigenetic state would result in the failure of stable

silencing of X-linked genes inactivated early on. It has been shown that a loss of DNA methylation is, in fact, confined to a subset of X-linked CpG islands (Gendrel et al., 2012), suggesting incomplete establishment of DNA methylation patterns. Although histone modifications in female MEFs homozygous for *Smchd1^{MD1}* were apparently indistinguishable from those in wild-type MEFs when examined by immunofluorescence microscopy, ChIP-seq analysis revealed that the distribution of H3K27me3 along the X chromosome was indeed locally affected. Genes de-repressed on the inactive X were often found in the regions manifesting a reduction in the enrichment of H3K27me3 relative to that in the wild type. Intriguingly, these genes belong to those characterized in a normal context by a lower enrichment of H3K27me3 in the ICM cells and trophectoderm at the blastocyst stage. This suggests that these de-repressed genes probably manage to undergo inactivation in the absence of H3K27me3 at the early stage of X inactivation but become de-repressed later on. It is tempting to speculate that SmcHD1 facilitates incorporation of H3K27me3 and perhaps other epigenetic modifications required for the stable maintenance of the X-inactivated state at later stages of X inactivation.

Another prominent effect caused by the lack of SmcHD1 is a failure to stably maintain the late replication state of the inactivated X chromosome. Although the X chromosome undergoing inactivation initially shifts its replication timing from early to late S phase as usual even in the absence of SmcHD1, the timing seems to revert earlier in the absence of SmcHD1. This is probably due to the failure to maintain late replication. The shift in replication timing could be a cause of de-repression of X-inactivated genes or a consequence of de-repressed genes being present on the inactive X chromosome. A gradual increase in the population of cells with two synchronously replicating X chromosomes over developmental stages implies that the latter might be the case. Although the X chromosome in these MEFs as a whole still displays properties of heterochromatin in terms of histone modifications, it is likely that this state of the modifications is insufficient for the maintenance of late replication of the inactivated X chromosome. In contrast, CRISPR/Cas9-meiodated disruption of the *Smchd1* gene resulted in neither a reversion of replication timing of the inactive X to early-mid S phase nor de-repression of X-linked genes in immortalized female MEFs. Given that X inactivation has been substantially established and stably maintained in wild-type female MEFs, it is likely that SmcHD1 is dispensable for the maintenance of the X-inactivated state once established to that extent. Taking all these findings together, we suggest that if SmcHD1 is not available during the process of X inactivation, the X chromosome fails to establish an appropriate chromatin state required for the stable maintenance of the X-inactivated state throughout successive cell divisions. Once this chromatin state is established with the involvement of SmcHD1, however, cells can manage to maintain such a chromatin state even if SmcHD1 is lost.

MATERIALS AND METHODS
Mice and genotyping

MommeD1 mice containing a point mutation at the *Smchd1* locus were previously described (Blewitt et al., 2008). They have been maintained by crossing heterozygotes with C57Bl/6 (B6) mice. The JF1 (*Mus musculus molossinus*) colony has been maintained in house. Mice carrying the *Xist^{ΔA}* allele were described previously (Hoki et al., 2009) and have been maintained by crossing female heterozygotes with B6 males. Females doubly heterozygous for *Xist^{ΔA}* and *Smchd1^{MD1}*, [X^{ΔA}X^{B6}; *Smchd1$^{MD1/+}$*], were produced by crossing X^{ΔA}X^{B6} females with *Smchd1$^{MD1/+}$* males, and males carrying X^{JF1} in combination with *Smchd1^{MD1}*, [X^{JF1}Y; *Smchd1$^{MD1/+}$*], were produced by crossing *Smchd1$^{MD1/+}$* males with JF1

females. These females and males were crossed to recover $X^{\Delta A}X^{JF1}$ and $[X^{\Delta A}X^{JF1}; Smchd1^{MD1/MD1}]$ fetuses, from which MEFs were prepared for RNA-seq. Genotyping of mice carrying $Smchd1^{MD1}$ and $Xist^{\Delta A}$ was carried out using primer sets listed in Table S1.

Cell culture
For generation of primary MEFs, E10.5 or E13.5 fetuses were minced by passing the trunk of the fetus (head and internal organs had been removed) through a 21-gauge syringe three times in 0.25% trypsin followed by pipetting using a P1000 Pipetman. Cells thus dissociated were cultured in Dulbecco's modified Eagle's medium containing 10% fetal bovine serum and penicillin/streptomycin.

Histology
E13.5 placentas fixed in Bouin's fixative were dehydrated, embedded in paraffin, sectioned at 6 μm and stained with Hematoxylin and Eosin.

TUNEL assay
E13.5 placentas fixed in 4% paraformaldehyde were dehydrated, embedded in paraffin, and sectioned at 6 μm. Paraffin sections thus produced were subjected to the TUNEL assay using an Apoptosis *in situ* Detection Kit (Wako Pure Chemical Industries) according to the manufacturer's instructions.

Replication timing assay
MEFs were labeled with 100 μg/ml 5-bromo-2-deoxyuridine (BrdU) for 9 h, in the presence of 40 μg/ml colcemid (Invitrogen) during the last 1 h of labeling. Metaphase spreads were prepared by a routine air-drying method and chromosomes were stained with freshly prepared Acridine Orange.

A typical late-replicating X chromosome looks pale along the entire region of the chromosome and bands representing the regions that have not incorporated BrdU and therefore have replicated early-mid S phase are almost invisible. Among the bands detected on the active X chromosome, the fourth band from the centromere was sometimes visible on the otherwise pale chromosome in wild-type female MEFs. We referred to an X chromosome showing this pattern as a late-replicating X. In a subset of mutant MEFs, we saw both X chromosomes exhibit multiple bands typically detected on an active X chromosome. Cells containing these X chromosomes were classified as those with two synchronously replicating X chromosomes even in the case in which one of them was slightly paler than the other.

RNA-FISH
Probes were labeled by nick translation in the presence of Green-dUTP (ENZO) or Cy3-dUTP (GE Healthcare) using pXistcDNA-SS12.9 and RP23-260I15 (*Atrx*) as templates. Cytological preparations of the embryonic ectoderm and trophoblast/extra-embryonic ectoderm were made as described previously (Takagi et al., 1982) and those of MEFs were made by the conventional air-drying method. Hybridization and subsequent washing were carried out as described previously (Sado et al., 2001).

Immunofluorescence
For immunofluorescence microscopy, MEFs grown on a coverslip were fixed with 0.4% paraformaldehyde for 10 min at room temperature, rinsed three times with PBS, and permeabilized for 10 min at room temperature in PBS containing 0.5% bovine serum albumin and 0.5% Triton X-100. Blocking was carried out in Blocking One (Nacalai Tesque) for 15 min at room temperature. The distributions of SmcHD1, H3K27me3, H2AK119ub, H3K9me2 and H4K20me1 detected using the antibodies described below were visualized using either Alexa Fluor 488-labeled (Invitrogen) or CF 594-labeled (Biotium) secondary antibodies against either mouse or rabbit IgG. Primary and secondary antibodies were diluted with Signal Enhancer HIKARI (Nacalai Tesque).

Antibodies
An antibody against SmcHD1 was generated by immunizing rabbits with a recombinant polypeptide corresponding to amino acids 800-1100 of SmcHD1 produced in *Escherichia coli*. The specificity of the antibody against SmcHD1

was validated by western blotting using whole cell lysate of MEFs prepared from wild type and Smchd1 homozygous mutants (Fig. S2A and Fig. 6A). The antibody was affinity purified using the recombinant polypeptide. Other antibodies used in this study were as follows: H3K27me3 (mouse monoclonal antibody; a gift from H. Kimura) (Hayashi-Takanaka et al., 2011), H2AK119ub (rabbit monoclonal antibody; Cell Signaling Technology, #8240S), H3K27me3 (rabbit polyclonal antibody; Millipore, 07-449), H3K9me2 (mouse monoclonal antibody; a gift from H. Kimura) (Kimura et al., 2008), H4K20me1 (mouse monoclonal antibody; a gift from H. Kimura) (Hayashi-Takanaka et al., 2015).

Allele-specific RNA sequencing (RNA-seq)
Total RNAs were extracted from MEFs using an ALLPrep DNA/RNA mini kit (Qiagen). Total RNA (1 μg) was subjected to enrichment for polyadenylated RNA, and libraries were prepared using a TruSeq stranded mRNA LT sample prep kit-set (Illumina) according to the manufacturer's instructions, and sequenced on an Illumina HiSeq to generate 101-nt paired-end sequence reads. Two biological replicate libraries each were prepared for $X^{\Delta A}X^{JF1}$ and $[X^{\Delta A}X^{JF1}; Smchd1^{MD1/MD1}]$ MEFs. Allele-specific RNA-seq analysis was performed as described by Sakata et al. (2017) with minor modifications: (1) paired-end reads were used as single-end reads; (2) the numbers of allele-specific reads in two replicates were summed; (3) genes with more than 20 allele-specific reads in both $X^{\Delta A}X^{JF1}$ and $[X^{\Delta A}X^{JF1}; Smchd1^{MD1/MD1}]$ were considered to be informative genes for assessing the expression of JF1 alleles. According to a generally accepted threshold (Peeters et al., 2014), genes with ≥ 10% of total expression from Xi in $X^{\Delta A}X^{JF1}$ were classified as escapees. To distinguish repressed genes from de-repressed genes in non-escapees, we set 10% of total expression from the Xi as a threshold. Allele-specific single-cell RNA-seq data of the pre-implantation and early post-implantation stage embryos were taken from GSE80810 and GSE89900, and processed as described by Borenszein et al. (2017a,b). Only embryos from B6 female×Cast male (BC) crosses were used for Fig. 5B.

ChIP-seq of H3K27me3
ChIP-seq was performed as described by Nozawa et al. (2013) with minor modifications. The sequence reads were aligned to the mouse reference genome (UCSC mm9, without Y chromosome) and a single unit of mouse ribosomal DNA repeats (BK000964.1). ChIP-seq reads in pre-implantation embryos (GSE73952) were aligned using bwa-mem (Li, 2013 preprint) and the biological replicates were pooled together for each stage following Liu et al. (2016). For Fig. 4A, we calculated H3K27me3 enrichment values defined as log2[(ChIP RPKM)/(Input RPKM)] in each non-overlapping 5-kb bin (RPKM: reads per kilobase per million mapped reads). We considered bins with Input RPKM <0.1 as unmappable and estimated their enrichment values by a linear interpolation of the closest mappable bins. For Fig. 4B and Fig. 5A, we calculated the H3K27me3 enrichment values in each X-linked gene body. Genes with length ≤1 kb or Input RPKM <0.1 were excluded due to low read counts.

Generation of *Smchd1* mutant immortalized MEF lines by CRISPR/Cas genome editing
A single-guide RNA (sgRNA) was designed using an online tool (http://crispr.mit.edu/). The immortalized MEFs were co-transfected with px330-U6-Chimeric_BB-CBh-hSpCas9 plasmid vector expressing both hSpCas9 and the sgRNA (Addgene plasmid #42230, deposited by Feng Zhang) (Cong et al., 2013) and a plasmid containing the puromycin resistance gene under the control of the mouse PGK promoter using FuGene HD transfection reagent (Promega, E2311). Two independent SmcHD1 mutants designated KO1 and KO2, respectively, were eventually obtained. The targeted region was amplified by PCR and sequenced using an Applied Biosystems (ABI) 3730 sequencer (Life Technologies) to determine the respective mutations.

ChIP-qPCR
ChIP was performed as described by Nozawa et al. (2013) using an antibody against H3K27me3. Primers used for qPCR are listed in Table S1.

Bisulfate sequencing

Genomic DNA was subjected to bisulfite-mediated C-to-U conversion and purified using EZ DNA methylation-Gold kit (Zymo Research). The converted DNA was used as a template for PCR and the amplified products purified using QIAquick PCR Purification Kit (Qiagen) were subsequently cloned into T-Vector pMD20 (Takara). Sequencing was carried out using at least 31 clones for each locus. Primer sequences used for bisulfate sequencing are listed in Table S1.

Author contributions

Conceptualization: K.N., T.S.; Methodology: K.N., T.S.; Validation: Y.S., K.N., T.S.; Formal analysis: Y.S., K.N., H.S., C.O., T.S.; Investigation: Y.S., K.N., T.S.; Resources: Y.S., M.B., T.S.; Data curation: K.N., T.S.; Writing - original draft: Y.S., K.N., T.S.; Writing - review & editing: Y.S., K.N., T.S.; Visualization: Y.S., K.N., T.S.; Supervision: T.S.; Project administration: T.S.; Funding acquisition: K.N., T.S.

Data availability

RNA-seq and ChIP-seq data were deposited in Gene Expression Omnibus under accession number GSE112097.

Supplementary information

Supplementary information available online at
http://dev.biologists.org/lookup/doi/10.1242/dev.166462.supplemental

References

Blewitt, M. E., Vickaryous, N. K., Hemley, S. J., Ashe, A., Bruxner, T. J., Preis, J. I., Arkell, R. and Whitelaw, E. (2005). An N-ethyl-N-nitrosourea screen for genes involved in variegation in the mouse. *Proc. Natl. Acad. Sci. USA* **102**, 7629-7634.

Blewitt, M. E., Gendrel, A.-V. V., Pang, Z., Sparrow, D. B., Whitelaw, N., Craig, J. M., Apedaile, A., Hilton, D. J., Dunwoodie, S. L., Brockdorff, N. et al. (2008). SmcHD1, containing a structural-maintenance-of-chromosomes hinge domain, has a critical role in X inactivation. *Nat. Genet.* **40**, 663-669.

Borenszteyn, M., Okamoto, I., Syx, L., Guilbaud, G., Picard, C., Ancelin, K., Galupa, R., Diabangouaya, P., Servant, N. and Barillot, E. et al. (2017a). Contribution of epigenetic landscapes and transcription factors to X-chromosome reactivation in the inner cell mass. *Nat. Commun.* **8**, 1297.

Borenszteyn, M., Syx, L., Ancelin, K., Diabangouaya, P., Picard, C., Liu, T., Liang, J.-B., Vassilev, I., Galupa, R. and Servant, N. et al. (2017b). Xist-dependent imprinted X inactivation and the early developmental consequences of its failure. *Nat. Struct. Mol. Biol.* **24**, 226-233.

Chadwick, B. P. and Willard, H. F. (2004). Multiple spatially distinct types of facultative heterochromatin on the human inactive X chromosome. *Proc. Natl. Acad. Sci. USA* **101**, 17450-17455.

Clemson, C. M., McNeil, J. A., Willard, H. F. and Lawrence, J. B. (1996). XIST RNA paints the inactive X chromosome at interphase: evidence for a novel RNA involved in nuclear/chromosome structure. *J. Cell Biol.* **132**, 259-275.

Cong, L., Ran, F. A., Cox, D., Lin, S., Barretto, R., Habib, N., Hsu, P. D., Wu, X., Jiang, W. and Marraffini, L. A. et al. (2013). Multiplex genome engineering using CRISPR/Cas systems. *Science* **339**, 819-823.

Corbel, C., Diabangouaya, P., Gendrel, A.-V., Chow, J. C. and Heard, E. (2013). Unusual chromatin status and organization of the inactive X chromosome in murine trophoblast giant cells. *Development* **140**, 861-872.

de Napoles, M., Mermoud, J. E., Wakao, R., Tang, Y. A., Endoh, M., Appanah, R., Nesterova, T. B., Silva, J., Otte, A. P. and Vidal, M. et al. (2004). Polycomb

group proteins Ring1A/B link ubiquitylation of histone H2A to heritable gene silencing and X inactivation. *Dev. Cell* **7**, 663-676.

Fang, J., Chen, T., Chadwick, B., Li, E. and Zhang, Y. (2004). Ring1b-mediated H2A Ubiquitination Associates with Inactive X Chromosomes and Is Involved in Initiation of X Inactivation. *J. Biol. Chem.* **279**, 52812-52815.

Gendrel, A.-V., Apedaile, A., Coker, H., Termanis, A., Zvetkova, I., Godwin, J., Tang, Y. A., Huntley, D., Montana, G. and Taylor, S. et al. (2012). Smchd1-dependent and -independent pathways determine developmental dynamics of CpG island methylation on the inactive X chromosome. *Dev. Cell* **23**, 265-279.

Hadjantonakis, A.-K., Cox, L. L., Tam, P. P. L. and Nagy, A. (2001). An X-linked GFP transgene reveals unexpected paternal X-chromosome activity in trophoblastic giant cells of the mouse placenta. *Genesis* **29**, 133-140.

Hayashi-Takanaka, Y., Yamagata, K., Wakayama, T., Stasevich, T. J., Kainuma, T., Tsurimoto, T., Tachibana, M., Shinkai, Y., Kurumizaka, H. and Nozaki, N. et al. (2011). Tracking epigenetic histone modifications in single cells using Fab-based live endogenous modification labeling. *Nucleic Acids Res.* **39**, 6475-6488.

Hayashi-Takanaka, Y., Maehara, K., Harada, A., Umehara, T., Yokoyama, S., Obuse, C., Ohkawa, Y., Nozaki, N. and Kimura, H. (2015). Distribution of histone H4 modifications as revealed by a panel of specific monoclonal antibodies. *Chromosome Res.* **23**, 753-766.

Heard, E., Rougeulle, C., Arnaud, D., Avner, P., Allis, C. D. and Spector, D. L. (2001). Methylation of histone H3 at Lys-9 is an early mark on the X chromosome during X inactivation. *Cell* **107**, 727-738.

Hoki, Y., Kimura, N., Kanbayashi, M., Amakawa, Y., Ohhata, T., Sasaki, H. and Sado, T. (2009). A proximal conserved repeat in the Xist gene is essential as a genomic element for X-inactivation in mouse. *Development* **136**, 139-146.

Hoki, Y., Ikeda, R., Mise, N., Sakata, Y., Ohhata, T., Sasaki, H., Abe, K. and Sado, T. (2011). Incomplete X-inactivation initiated by a hypomorphic Xist allele in the mouse. *Development* **138**, 2649-2659.

Holliday, R. and Pugh, J. E. (1975). DNA modification mechanisms and gene activity during development. *Science* **187**, 226-232.

Jeppesen, P. and Turner, B. M. (1993). The inactive X chromosome in female mammals is distinguished by a lack of histone H4 acetylation, a cytogenetic marker for gene expression. *Cell* **74**, 281289.

Keniry, A., Gearing, L. J., Jansz, N., Liu, J., Holik, A. Z., Hickey, P. F., Kinkel, S. A., Moore, D. L., Breslin, K. and Chen, K. et al. (2016). Setdb1-mediated H3K9 methylation is enriched on the inactive X and plays a role in its epigenetic silencing. *Epigenetics Chromatin* **9**, 16.

Kimura, H., Hayashi-Takanaka, Y., Goto, Y., Takizawa, N. and Nozaki, N. (2008). The organization of histone H3 modifications as revealed by a panel of specific monoclonal antibodies. *Cell Struct. Funct.* **33**, 61-73.

Kohlmaier, A., Savarese, F., Lachner, M., Martens, J., Jenuwein, T. and Wutz, A. (2004). A chromosomal memory triggered by Xist regulates histone methylation in X inactivation. *PLoS Biol.* **2**.

Leong, H. S., Chen, K., Hu, Y., Lee, S., Corbin, J., Pakusch, M., Murphy, J. M., Majewski, I. J., Smyth, G. K. and Alexander, W. S. et al. (2013). Epigenetic regulator Smchd1 functions as a tumor suppressor. *Cancer Res.* **73**, 1591-1599.

Li, H. (2013). Aligning sequence reads, clone sequences and assembly contigs with BWA-MEM. *arXiv:1303.3997*.

Liu, X., Wang, C., Liu, W., Li, J., Li, C., Kou, X., Chen, J., Zhao, Y., Gao, H. and Wang, H. et al. (2016). Distinct features of H3K4me3 and H3K27me3 chromatin domains in pre-implantation embryos. *Nature* **537**, 558-562.

Lyon, M. F. (1961). Gene Action in the X-chromosome of the Mouse (Mus musculus L.). *Nature* **190**, 372-373.

Marahrens, Y., Panning, B., Dausman, J., Strauss, W. and Jaenisch, R. (1997). Xist-deficient mice are defective in dosage compensation but not spermatogenesis. *Genes Dev.* **11**, 156-166.

Nozawa, R.-S., Nagao, K., Igami, K.-T., Shibata, S., Shirai, N., Nozaki, N., Sado, T., Kimura, H. and Obuse, C. (2013). Human inactive X chromosome is compacted through a PRC2-independent SMCHD1-HBiX1 pathway. *Nat. Struct. Mol. Biol.* **20**, 566-573.

Panning, B. and Jaenisch, R. (1996). DNA hypomethylation can activate Xist expression and silence X-linked genes. *Genes Dev.* **10**, 1991-2002.

Peeters, S. B., Cotton, A. M. and Brown, C. J. (2014). Variable escape from X-chromosome inactivation: identifying factors that tip the scales towards expression. *BioEssays* **36**, 746-756.

Penny, G. D., Kay, G. F., Sheardown, S. A., Rastan, S. and Brockdorff, N. (1996). Requirement for Xist in X chromosome inactivation. *Nature* **379**, 131-137.

Plath, K., Fang, J., Mlynarczyk-Evans, S. K., Cao, R., Worringer, K. A., Wang, H., de la Cruz, C. C., Otte, A. P., Panning, B. and Zhang, Y. (2003). Role of histone H3 lysine 27 methylation in X inactivation. *Science* **300**, 131-135.

Sado, T., Wang, Z., Sasaki, H. and Li, E. (2001). Regulation of imprinted X-chromosome inactivation in mice by Tsix. *Development* **128**, 1275-1286.

Sakata, Y., Nagao, K., Hoki, Y., Sasaki, H., Obuse, C. and Sado, T. (2017). Defects in dosage compensation impact global gene regulation in the mouse trophoblast. *Development* **144**, 2784-2797.

Schotta, G., Sengupta, R., Kubicek, S., Malin, S., Kauer, M., Callen, E., Celeste, A., Pagani, M., Opravil, S. and De La Rosa-Velazquez, I. A. et al. (2008). A chromatin-wide transition to H4K20 monomethylation impairs genome integrity and programmed DNA rearrangements in the mouse. *Genes Dev.* **22**, 2048-2061.

Silva, J., Mak, W., Zvetkova, I., Appanah, R., Nesterova, T. B., Webster, Z., Peters, A., Jenuwein, T., Otte, A. P. and Brockdorff, N. (2004). Establishment of histone H3 methylation on the inactive X chromosome requires transient recruitment of Eed-Enx1 polycomb group complexes. *Dev. Cell* **4**, 481-495.

Takagi, N. and Sasaki, M. (1975). Preferential inactivation of the paternally derived X chromosome in the extraembryonic membranes of the mouse. *Nature* **256**, 640-642.

Takagi, N., Sugawara, O. and Sasaki, M. (1982). Regional and temporal changes in the pattern of X-chromosome replication during the early post-implantation development of the female mouse. *Chromosoma* **85**, 275-286.

Wang, J., Mager, J., Chen, Y., Schneider, E., Cross, J. C., Nagy, A. and Magnuson, T. (2001). Imprinted X inactivation maintained by a mouse Polycomb group gene. *Nat. Genet.* **28**, 371-375.

Wutz, A. (2011). Gene silencing in X-chromosome inactivation: advances in understanding facultative heterochromatin formation. *Nat. Rev. Genet.* **12**, 542-553.